International Journal of Architectural Heritage, 5: 1–32, 2011

ISSN: 1558-3058 print / 1558-3066 online
DOI: 10.1080/15583050903367595

Taylor & Francis
Taylor & Francis Group

THREE-DIMENSIONAL ANALYSIS OF MASONRY VAULTS USING LIMIT STATE ANALYSIS WITH FINITE FRICTION

D. F. D'Ayala[1] and E. Tomasoni[2]

[1]*Department of Architecture and Civil Engineering, University of Bath, Bath, UK*
[2]*Dipartimento di Ingegneria Civile, Architettura, Territorio e Ambiente, (DICATA), Universita' di Brescia, Brescia, Italy*

Within the past 20 years, a growing number of methods for the analysis of masonry vaults have been developed. However, most methods idealize the vaults as a system of many arches. This oversimplification could be admissible for barrel vaults and spherical domes under simple gravitational loads, but it cannot do justice to the three-dimensional effects developing in other types of vaults, especially in complex vaults without smooth and continuous surface. Moreover, although the results could be conservative for uniform load distributions, this model limits substantially the set of loading conditions that can be analyzed and hence provide an accurate assessment of vaults performance. To clear this limitation, this article proposes a tool for three-dimensional analysis of masonry vaults. Using the lower bound approach and taking into account the friction among block interfaces, the proposed analytical method may give a good indication of the actual surface of thrust within the framework of limit state analysis. Therefore, limit state analysis with finite friction is able to provide the crack pattern, the stress resultants and the horizontal thrust at the supports, important elements with regard to strengthening interventions. To show its simplicity and rigor, the procedure has been applied to pavilion vaults. The results obtained are validated by comparison with nonlinear finite element analysis and an application to a real case study is presented.

KEY WORDS: vaults, pavilion vaults, friction, limit analysis, masonry

1. INTRODUCTION

Masonry vaults and domes are some of the main structural features of architectural heritage. Therefore, the assessment of their structural safety and the determination of their stress field is a very important task for preservation of historic buildings. Over the years, different approaches have been developed to analyze masonry vaults: plasticity analysis using the line of thrust method (Heyman 1966; Harvey 1988; Huerta 2001), membrane theory (Heyman 1966; Flügge 1975), and force network model, i.e. Pucher's approach (O'Dwyer 1999). Furthermore, the development of constitutive laws for masonry structures has led to extensive application of finite element (FE) analysis to the assessment of vaulted structures (Lourenço 2001; Cattari et al. 2008).

In the framework of the FE method, two main approaches are usually considered: the continuum approach, based on the homogenization theory (Lourenço 1996; Calderini

Received 21 December 2008; accepted 27 September 2009.
Address correspondence to D. F. D'Ayala, Senior Lecturer, Department of Architecture and Civil Engineering, University of Bath, Bath, BA2 7AY, UK. E-mail:

& Lagomarsino 2006), and the discrete approach, based on the separate modeling of blocks and mortar, where the blocks are modeled using conventional continuum elements, either linear or non-linear, and the joints are represented by interface or contact elements (Lourenço & Rots 1997).

Although the discontinuities can be incorporated by use of smeared crack model or contact elements, the most effective approach to analyze masonry structures is the use of distinct element method (DEM), that consider the structure as a series of distinct blocks interacting through unilateral elastoplastic contact conditions. This discrete approach, initially developed by Cundall (1971) for rock mechanics, was subsequently applied to dry block masonry by Amadei (1995), Lemos (1997), and Mirabella et al. (1998). This approach is particularly useful to analyze cases in which displacement are significant and concentrated at interfaces. The limitation of this technique lies in its high computational burden when meaningful structural models are considered.

Hence, the application of limit analysis theory to masonry, as developed by Heyman, is often considered as the best tool for the analysis of masonry arches and vaults (Huerta 2001; Baggio & Trovalusci 1998). It indeed presents a useful and intuitive approach to understand the behavior of arches and vaults and provides the value of minimum thickness to span ratio as a safe solution under the assumptions of infinite compressive strength, infinite friction resistance, and zero tensile strength.

For Heyman (1966), the actual stress state cannot be found, but to establish a safety criterion is what matters. In the spirit of 'standard' limit analysis, all methods able to give an admissible stress state can be used to give a lower bound of the collapse load. Geometry and loading are the basic input data. In this approach, the possibility of sliding is ruled out *a priori*. However cracking is considered and limit configurations able to assure the equilibrium after cracking are identified (Heyman 1977).

In real vaults however, sliding does occur, especially if accompanied by a loss of shape. In that case, neglecting the sliding failure mode, may lead to unsafe estimates of the solution. Stereotomy of the vault, coefficient of friction and resistance to tension must then be considered (D'Ayala 1993; 1994). D'Ayala & Casapulla (2001) use the knowledge of extreme meridian normal forces in a dome to demonstrate its stability, even in the case of potential sliding. Smars (2000) showed that locally stronger structures are not necessarily safer, proposing a technique to build a lower bound domain for structures having possible local tension resistance. Moreover, the author demonstrates the importance of defining minimal normal forces on the joint and tries to quantify these forces (Smars 2008).

Livesley (1978; 1992), by adopting a static approach, was the first to develop a formal linear programming procedure to discuss the existence of safe load factor of two-dimensional vaulted structures. Within this approach research has developed substantially in the past decade (D'Ayala,1993; Boothby 1994; Baggio & Trovalusci 1998; Ferris & Tin Loi 2001).

Besides the sliding issue, it is also very important to take into account three-dimensional (3D) effects. Heyman's () work suggests that, for complex vaults, connections between shell surfaces are loci of stress concentrations and particularly of development of tensile and shear state of stress due to difference in stiffness. The difficulty inherent in resolving the 3D differential problem that ensue, often leads to a reduction to a simplified system of separate arches. While this simplification, apparently in agreement with the safe theorem of plasticity, could be admissible for barrel vaults and spherical domes under gravitational loads, cannot do justice of the 3D state of stress developing in other more

complex vaults, ribbed or with discontinuity lines. Such effects may be essential to explain stability or may represent critical stress zones leading to unsafe conditions.

O'Dwyer (1999) has taken into account redistribution effects, modeling the principal stresses in a masonry vault as a discrete network of forces (Pucher's approach). However this work assume an initial value for the horizontal component of the resultant of stresses under the condition that the friction between the voussoirs is sufficient to prevent failure due to sliding.

On the basis of this work, Andreu et al. (2007) present a computer technique for the assessment of complex masonry constructions. This method simulates numerically a network of forces in equilibrium that represents the thrust lines of the structure in an inverted model. By means of an optimization process, the Andreu's computational formulation allows to assess the safety of masonry structures and to evaluate their ultimate capacity. Nevertheless, this procedure does not take into account the sliding mechanisms.

Using the same method, founded on projective geometry, duality theory and linear optimization, Block and Ochsendorf (2008) propose an interactive design tool for finding 3D equilibrium of compression-only surfaces. This interesting tool allows the investigator to assess the stability of masonry vaults with complex geometries. Nevertheless, by means of this methodology, the sliding mechanism cannot occur and stress redistribution after cracking is not taken into account. These limitations mean that the method, perfect for the design of new vaulted structures, could be not sufficiently accurate for the analysis and the control of safety levels of historic vaults.

Both the 3D effects and the sliding mechanism are analyzed by D'Ayala & Casapulla (2001).This study proposes a tool based on the limit state approach for the analysis of hemispherical domes. Identifying a thrust surface and taking into account the limited friction between the blocks, the authors provide a simple proof of the unique solution and show how friction might affect the failure mechanism in a spherical dome.

Moving from the same assumptions of D'Ayala & Casapulla (2001), the present work generalize the application of this procedure to vaults of more complex geometry, for which the 3D state of stress cannot be reduced by assumption of axial symmetry. In particular, limit state analysis with finite friction is applied to masonry pavilion vaults, in order to evaluate structural behavior, crack pattern, stress field and minimum thickness to define the stability condition, all essential aspects when designing structural rehabilitation intervention. The validity of the approach is demonstrated by comparing the results obtained with nonlinear FE analysis simulations. The application to a case study concludes this article.

2. EQUILIBRIUM CONDITIONS ON THREE-DIMENSIONAL INTERFACES WITH FINITE FRICTION

Usually, the constitutive model for a masonry material is based on the assumptions introduced by Heyman () of infinite compressive strength for the blocks, no tension transmitted across the joints and absence of sliding failure. Based on these hypotheses, possible failure is confined to rotation of blocks. However, vaults with shallow profiles, or made of tuff or sandstone blocks without mortar, or with concentrated loads may fail by way of sliding.

For this reason, it is essential to relax the hypothesis relative to the frictional behavior of the material and to deal with the nonassociative nature of the resulting constitutive

law. Indeed, especially for historical structures, due to deterioration of contact surfaces or of binding materials, the original friction coefficient could be substantially reduced and sliding mechanism can occur, especially when lateral loads are also present, such as wind or seismic action. Therefore, assuming the Coulomb criterion as a good representation of the real behavior, the shear strength at blocks interfaces is not infinite, but determined by the cohesion and the internal friction angle. This assumption is supported by few tests performed on historic masonry to quantify both characteristic shear strength and friction coefficient.

Vasconcelos and Lourenço (2006) present an extensive experimental research on stone masonry walls reproducing historic materials. This work shows that the shear strength of the walls can be predicted by the Coulomb criterion and values of the friction coefficient lower than 0.4 are common in historic masonry. Other experimental results, performed by direct shear tests, reported by Atkinson et al. (1989) on old masonry, by Magenes (1992) on bricks with lime mortar and by Mirabella and Calvetti (1997) on bricks with hydraulic lime mortar, provide value of friction coefficient in the region of 0.6. Nevertheless yearly temperature cycles can lead over a few centuries to deterioration of the bed joint surfaces or of the binding materials, resulting in substantial reduction of the friction coefficient as shown by Lourenço and Ramos (2004) that proposes experimental tests in direct shear for dry masonry joint.

Hence, modeling a vault as a 3D discrete system of rigid blocks, each portion identified by the intersection of two parallels with two adjacent meridians can be considered as a macroelement of homogenous masonry material, with infinite internal compression, limited tensile strength and shear strength at the interfaces between portions defined by a Coulomb criterion. To determine the stress field in the vault, as the weaker elements in the fabric are the joints, the analysis can be most usefully carried out at the blocks' interfaces, where failure by shear or tension will first occur.

Figure 1 shows the geometric parameters used to identify the generic interface surface and the stress resultants for a generic state of stress on a block interface for a pavilion vault. The interface is identified by a meridian angle θ_j and a parallel angle α_p (Figure 1a). S_j is the meridian resultant of stress at interface j, not necessarily normal to the interface surface (Figure 1c). This implies that through-depth shear arise on the interface and hence the pure membrane conditions are not applicable any more. Furthermore each block will also be subjected to hoop stresses H_p and in plane shear $T_{x\theta\, p}$ at meridian interfaces and its reciprocal $T_{x\, j}$ at parallel interfaces.

Considering for simplicity equilibrium to gravity loads only, the generic state of stress reduces to component S_j and H_p, and hence this reduces to an isostatic problem. This simplification is initially considered to prove the safety and uniqueness of the solution. In this condition, the two stresses resultant for a portion of vault identified by the angles α and θ and its weight are all contained in a vertical plane and can be represented as in Figure 2. By drawing at the interface the projection of the cohesion-less Coulomb cone identified by an angle of friction $|\varphi|>0$ it is immediate to see that the range of admissible values for the stress resultant S_j has a lower bound depending on the weight and the amplitude of the angle of friction φ:

$$Sj \geq S_{Lim} = \frac{W_j}{\sin(\theta_j + \varphi)} \tag{1}$$

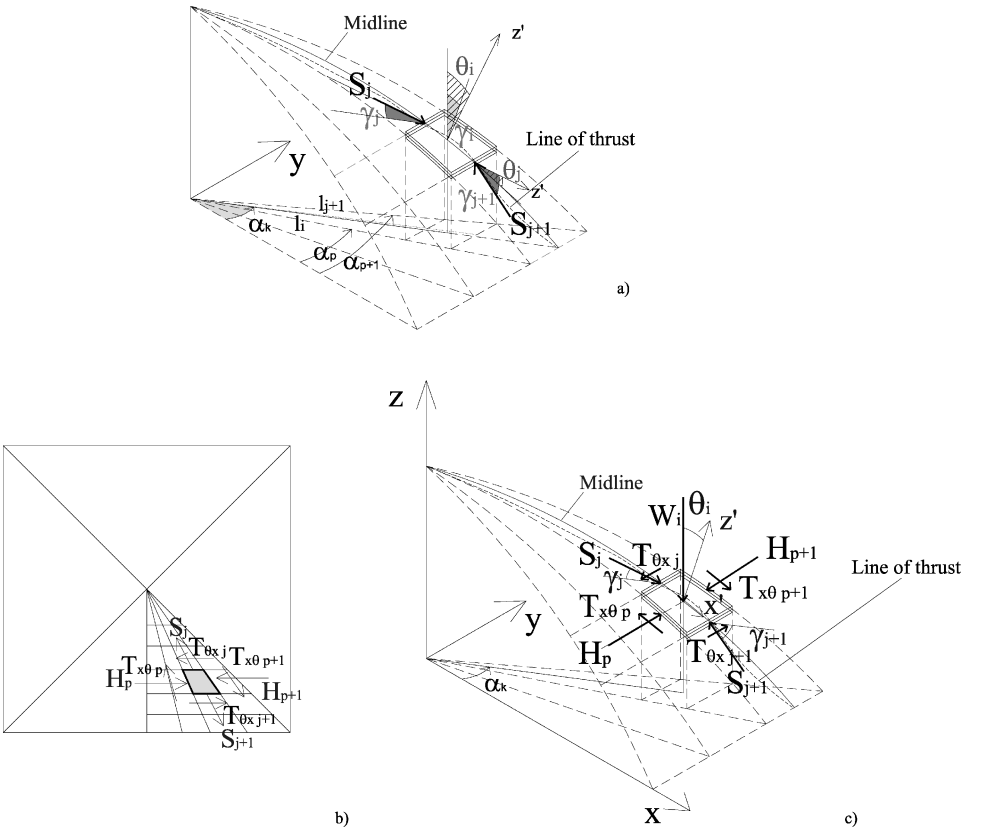

Figure 1. Axonometric view of a pavilion vault with the representation of (a) the geometric parameters used to identify the generic interface surface; (b) view from above, and (c) axonometric view with the representation of the resultants of forces on a generic element.

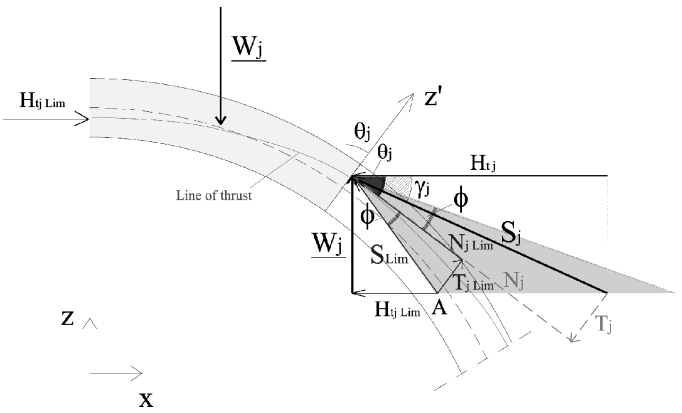

Figure 2. Representation of forces *Nj* and *Tj*, components of *Sj* normal and parallel to the interface *j* respectively, and Coulomb's cone projection, for an angle of friction *f*. The equilibrium limit condition for the applied load is also shown.

where the equality defines point A on the Coulomb's cone projection (Figure 2), implying the incipient outward sliding of the lower portion of the vault with respect to the upper one. The shape of the structure and the assumption of rigid bodies prevent the opposite direction of sliding, unless a lateral displacement at the support occurs.

The limiting value of compressive and shear force resultants are statically defined and can be obtained by taking components of the stress resultants S_{Lim} in the directions normal and tangential to the meridian, as follows:

The limiting values of T_j and N_j given by relations in Equation (2) are independent of each other and only depend on the self-weight and on the given value of φ. This means that, in case of gravity loading, there is a unique limiting value of the shear force, and the local equilibrium problem is at a limit state statically determined. This derives from the fact that, even for non standard materials, if normal forces are given at a limit state (conditions in Equation [2]), then they can be ignored in defining the yield surface, and, consequently, the Coulomb's cone reduces to a circle in the plane of shear forces. The problem of applicability of plasticity theory to non-conforming materials was first address by Drucker (1954). The existence of safe solutions under these conditions was first proven by Palmer (1966) and De Josselin de Jong (1964) with reference to soils. Later, Livesley (1978) and Michalowski and Mroz (1978) showed application to arched structures and mechanical contact problems, respectively, also showing that associative flow rules leads to overestimates of the solution. The size of the Coulomb failure domain in the shear plane depends on the magnitude of the normal force, but the imposition of the normality rule now does not implies dilatancy, as the flow is all contained in the associated shear deformation plane, and hence the solution, being equilibrated, at the yield surface, and not violating the kinematical constraints, is indeed the correct solution and is unique. Therefore the material constraints become now standard and the analysis falls within the framework of the classical plasticity theory.

Relaxing the condition of gravity loads will imply that in depth shear will generally arise. However as this lies in a plane normal to the component *Nj*, it will only affect the direction and magnitude of the shear stress resultant and not its limiting value. The Coulomb criterion can hence be written as:

$$\sqrt{T_j^2 + T_{\theta x}^2} \leq T_0 + N_j \mu \tag{3}$$

where T_0 is a finite cohesion and generalizes the argument developed in the previous paragraph for cohesion-less materials. If the tangential resultant shear force exceeds the limit in Equation (3), the vault could fail by way of sliding. The issue then remains of identifying, direction, magnitude and point of application of S_j.

As it can be seen from Figure 2, for the same value of W_j and variable H_{tj} (resultant horizontal trust), S_j can assume different directions and magnitudes, limited by the range shown in this equation:

$$\left|\gamma_j - \theta_j\right| \leq \phi \tag{4}$$

Furthermore also its point of application, i.e. the distance between the surface of trust and the median surface of the vault at any point is not predetermined, but is also constrained by the condition that the material does not resist tensile action. This implies that, according to Heyman the surface of trust is entirely contained within the thickness t of the vault, or,

in other words, is completely bounded by its intrados and extrados surfaces. This condition can be expressed as follows:

$$e_j = \Delta R_j = \left| R_j^{geom} - R_j^t \right| \leq \frac{t}{2} \tag{5}$$

where e_j is the eccentricity of the trust surface with respect of the median surface at the point of application of S_j, the meridian stress resultant, R_j^{geom} is the distance of the median shell surface from the origin of the coordinate and R_j^t is the distance of the thrust surface form the origin of coordinate. Hence, these conditions in Equations (4) and (5) can be combined in a single compatibility condition

$$\mathbf{E}(\alpha_p, \theta_j) \geq \mathbf{T}(\alpha_p, \theta_j, \phi) \geq \mathbf{I}\left(\alpha_p, \theta_j\right) \tag{6}$$

i.e., the thrust surface ***T*** is bounded at the same time by the intrados surface ***I*** and extrados surface ***E*** and conditioned by the Coulomb criterion defined by Equations 3 and 4. In Equation (6) global polar coordinates are used in preference to linear coordinates to emphasize the importance of curvature and inclination to the vertical identifying the surface of thrust ***T*** that satisfies at the same time both equilibrium condition, compatibility and material constraints.

The problem of defining the thrust surface can then be formally set in terms of a series of equilibrium equations for each of a number of blocks in which the vault can be discretized and the thrust surface linearized, conditioned by the material and compatibility constraint defined in Equations (4) and (5). As both constraint conditions and equilibrium equations are linear, the problem can be formally set in terms of linear programming and an optimized solution can be sought as shown in Livesley (1992) and D'Ayala (1994). In this case, Equation (5) can be chosen as the target function. This choice is particularly appropriate because the definition of the minimum necessary thickness to contain the thrust surface respond to one of the corollaries of the safe theorem of plasticity. Because the problem is set in terms of linear programming, it is a convex and constrained problem and hence the optimized solution is a global minimum. The approach is in the framework of a lower bound and this, as proved by other authors, in the case of nonassociative flow rule may lead to underestimates of the structural capacity. For this reason the results are validated against a FE nonlinear model as presented in section 4 of this paper. A more generalized approach, which takes into account the interaction effects of shear, torsion and bending, and the loading history, for walls assemblies, is presented by Orduna and Lourenço (2005a; 2005b). The procedure is developed for electronic spreadsheet and a multipurpose mathematical programming solver is used to solve the problem of optimum.

In the following text, an application to pavilions vault is presented showing the detailed development of the equilibrium, compatibility, and constraint conditions, formulated at the level of the single block, and how these relate to the global conditions as previously presented. In particular the change in stress resultant and the effect on the line of thrust of the meridian cracks is highlighted. Before this discussion, an introduction on the development of pavilion vaults in architectural history is presented to outline the practical relevance of the analytical tool.

3. APPLICATION TO MASONRY PAVILION VAULTS

3.1. Introduction

Pavilion vaults were already used in Roman architecture from the first century BC (for example, in Tabularium, 78 BC; Domus Aurea, 64–68 BC; and Domus Augustana, 81–92 BC; and later in Diocletian's Baths, 298–306 AD). Despite the substantial changes in materials and building techniques, the shape was still widely in use in post-imperial Italy. Indeed, in early Christian Italian architecture, masonry pavilion vaults were built to cover polygonal churches, chapels and baptisteries (for example, St. Aquilino in Milan, 5th century AD, and the Aryan baptistery, 6th century AD). Furthermore, in Romanesque architecture this type of vaults was found at the intersection between the transept and the church nave (for example, St. Ambrogio in Milan and St. Michele in Pavia). The most substantial application of pavilion vaults, however, is associated with the development of the Renaissance palace from the beginning of the 16th century. Numerous examples of pavilion vaults are also present in Ottoman architecture from the 18th century onwards, used mainly as soffits in rectangular spaces.

Despite their common use in the past centuries, masonry pavilion vaults have not been the subject of accurate structural analysis, notwithstanding the many instances of failures and need for repair or strengthening. The main reason for this apparent lack of interest is their singularity of shape and presence of cusps along the diagonal, which leads to a complex 3D state of stress, even under uniform gravity loads, not easily studied by simplified approaches (Tomasoni 2008).

This type of vaults is often affected by cracks along the diagonals (Figure 3), where the geometry of the vault is farthest from the geometry of the thrust surface generated from the gravity load distribution. Cracks might also develop toward the centre of the web of each portion so, in the past, they have often been modeled as independent arches (Cangi 2005). However, the simplified arch model, does not account for the capacity of the vault to transfer load associated with shear and for the arch effect that can be develop

Figure 3. Photograph of pavilion vaults of Martinengo delle Palle's palace (Brescia, Italy), where diagonal cracks can be seen.

within the horizontal strips due to their non negligible thickness, similarly to the arch effect accounted for in walls or slabs. Overlooking redistribution of stress resultants due to shear stiffness leads to an incorrect quantification and location of the maximum level of thrust on the vault's supporting walls, and does not allow quantifying the extension of cracking along the diagonal or other meridians.. Accurate estimates of both phenomena is however essential for a sound design of strengthening intervention by way of anchors insertion or frp strip bonding.

In the following section is shown how an application of the procedure outlined above to a typical pavilion vault, is able to provide more reliable answers to the determination of a geometric safety factor for the vault, which can be expressed, as proposed by Heyman as the ratio between the geometric thickness over the minimum required thickness; and the accurate position of hinges and sliding surfaces at failure, leading to better positioning of anchors or other thrust contrasting devices. The validation of the implemented optimization routine is carried out by comparison first with results obtained with a FE nonlinear simulation, and then with a real case 17th-century vault.

3.2. Formulation of the Static Problem Suitable for Spreadsheet Programming

The simplest and most frequent occurrence, according to the technical literature (Scamozzi 1964 [1615]; Levi 1932), is a pavilion vault over a plane square area, generated by a semicircular arch at the centre of the web and subject to self-weight loading (Figure 4). Considering a pavilion vault with generatrix radius R, vault rise f, span l and thickness t (Figure 4b), the procedure is developed for a half sector. As shown in Figure 4a, according to historic technical literature, the diagonal ribs and any arch except the midspan one, can be described by the equation of an ellipsis (Curioni 1870; Breymann 2003; Levi 1932).

Assuming the n slices are made up of m blocks, each block is identified, in a global Cartesian system with origin at the centre of the horizontal projection of the vault, by the coordinates of its centre of mass:

$$x_i^{geom} = R \cdot \sin \underline{\theta_i} \tag{7}$$

$$y_i^{geom} = R \cdot \sin \underline{\theta_i} \tan \alpha_k \tag{8}$$

$$z_i^{geom} = R \cdot \cos \underline{\theta_i} \tag{9}$$

for $i = 1$ to m and k=1 to n (Figure 5). In (Equation 7) to (Equation 9) R is the constant radius of the generatrix, $\underline{\theta_i}$ is the angle between the vertical and perpendicular to the generatrix, $\alpha_k$is the angle between the **X** global axis and the projection of the generatrix on the horizontal plane as shown in Figure 5a.

The relation between θ_i and $\underline{\theta_i}$ is:

$$\tan \underline{\theta_i} = \tan \theta_i \cdot \cos \alpha_k \tag{10}$$

As discussed in section 2 the identification of the position of a sufficient number of points representative of the thrust surface completely defines the static problem and its solution. The strategy adopted is to define the coordinates of such points in terms of the

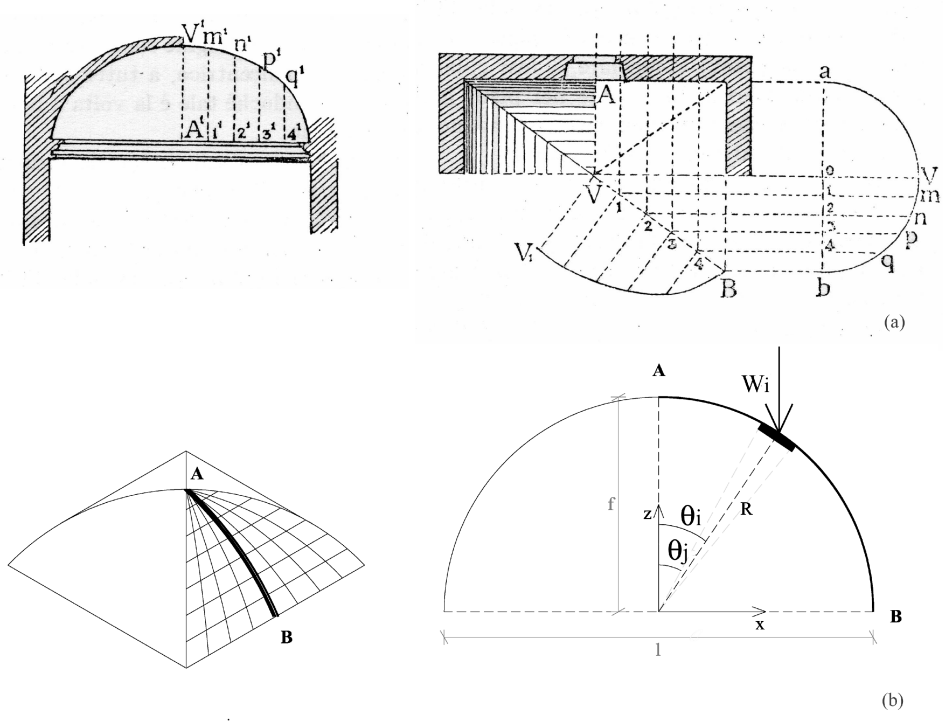

Figure 4. Schematic illustrations of (a) the geometric characteristic of the diagonal and of the vault's generatrix by historic technical literature (Levi, 1932), and (b) geometric parameters of the vault's generatrix adopted for the analysis.

difference with respect to the coordinates of equivalent point on the median surface of the vault. As the loading condition assumed is purely gravitational, the first step consists in defining the geometry of the thrust surface by determining the relationship between the coordinates of its representative point within a block and the centre of gravity of that block:

$$x_i^t = x_i^{geom}, \quad y_i^t = y_i^{geom}, \quad z_i^t = z_i \tag{11}$$

indicating that the coordinate $z_i{}^t$ is the chosen unknown.

However it is more relevant to define the coordinates of a representative point on the interface as this is where the equilibrium conditions and geometric constraint need to be satisfied. From simple linear proportion:

$$\left|z_i^t - z_j^t\right| = \left|l_i^t - l_j^t\right| \cdot \tan\gamma_j \tag{12}$$

where with reference to Figure 5, $l_j{}^t$ is the horizontal component of the distance between the interface and the origin of the global reference system and $l_i{}^t$ is the horizontal projection of the distance between the centre of block and the origin of the global reference system. Hence, the coordinates of a generic point of the thrust surface at the interface can be derived as follows:

$$z_j^t = \frac{z_i^t + \frac{x_i^t}{\cos\alpha_k} \cdot \tan\gamma_j}{1 + \frac{\tan\theta_j}{\cos\alpha_k} \cdot \tan\gamma_j} \tag{13}$$

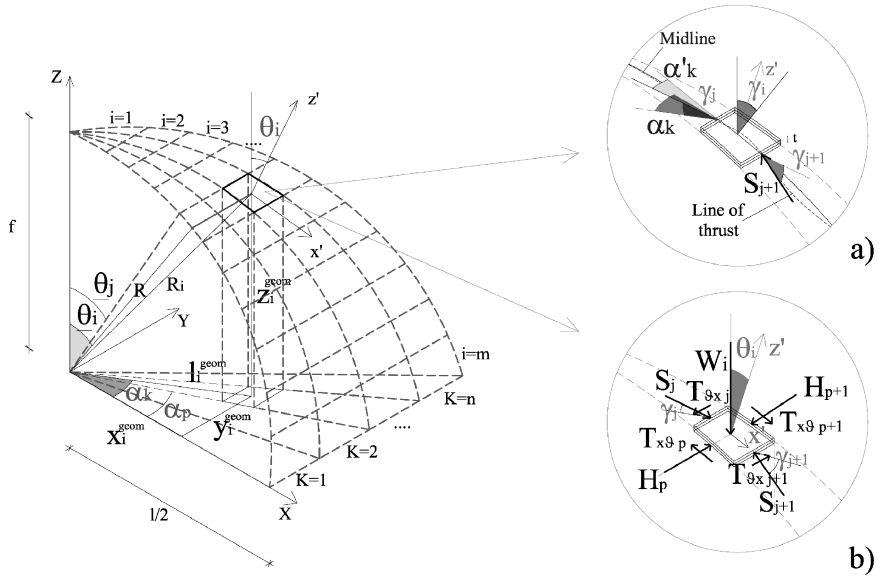

Figure 5. Schematic illustrations of the axonometric view of pavilion vault, with (a) the representation of the angles γ_i and α'_k (a) and (b) representation of the gravitational load and stress resultants for a generic element.

$$x_j^t = z_j^t \cdot \tan \underline{\theta_j} \text{ and } y_j^t = R_i^t \cdot \sin \underline{\theta_j} \tan \alpha_k \tag{14}$$

with:

$$l_j^t = z_j^t \cdot \frac{\tan \underline{\theta_j}}{\cos \alpha_k} \tag{15}$$

and:

$$\gamma_j = \arctan \left| \frac{z_{i+1}^t - z_i^t}{l_{i+1}^t - l_i^t} \right| \tag{16}$$

With reference to Figure 5, considering equilibrium along the local vertical axis **z'** normal to the vault surface at the centre of the element, subjected to its own weight, the 330
meridian force S_j can be written as:

$$S_j = \frac{-W_i \cdot \cos \gamma_i}{\sin(\gamma_i - \gamma_j) + \sin(\gamma_{j+1} - \gamma_i)} \tag{17}$$

where second order terms have been neglected in deriving the equilibrium equation.

The weight W_i of each block identified by meridian angles θ_j and θ_{j+1} and by the parallel angles α_p and α_{p+1} can be calculated as follows:

$$W_i = \rho \cdot t \cdot \int_{\underline{\theta_j}}^{\underline{\theta_{j+1}}} \int_{y_p}^{y_{p+1}} R \, d\underline{\theta} \, dy = \rho \cdot t \cdot \int_{\underline{\theta_j}}^{\underline{\theta_{j+1}}} R^2 \cdot \sin \underline{\theta} \cdot (\tan \alpha_{p+1} - \tan \alpha_p) \, d\underline{\theta} \tag{18}$$

If the vault is subdivided in n slices of equal aperture $\Delta\alpha$, for a vault over square base area, the resultant gravity load for each element is:

$$W_i = \rho \cdot t \cdot R^2 \left(\cos \underline{\theta_j} - \cos \underline{\theta_{j+1}}\right) \cdot \left(\tan \alpha_{p+1} - \tan \alpha_p\right) \tag{19}$$

Next, the shear force $T_{x\theta}$ at the interface between two slices can be quantified using translation equilibrium along the **x'** axis of the local system:

$$T_{x\theta\ p+1} = S_j \cdot \cos(\gamma_i - \gamma_j) - S_{j+1} \cdot \cos(\gamma_{j+1} - \gamma_i) - W_i \cdot \sin \gamma_i + T_{x\theta\ p} \tag{20}$$

where the subscript p indicate the lateral surface of the generic block.

Given the symmetry of the problem for self weight, for the interface $p=0$ between the slices at the centre of the web, corresponding to y=0, the shear resultant $T_{x\theta}$ =0. Hence, using rotation equilibrium around the **z'** axis (Figure 5b), the shear resultant $T_{\theta x}$ at a location different from midspan is:

$$T_{\theta x\, j+1} = \frac{\left(T_{x\theta\ p} + T_{x\theta\ p+1}\right) \cdot \cos \alpha'_k \cdot \sin \theta_i \cdot \left(tg\alpha_{p+1} - tg\alpha_p\right)}{\theta_{j+1} - \theta_j} - T_{\theta x\, j} \tag{21}$$

where the angle α'_k is the angle α_k projected in the plane tangent to the thrust surface at the centre of element (see figure 5a):

$$\alpha'_k = \arcsin\left(\cos \gamma_j \cdot \sin \alpha_k\right) \tag{22}$$

The in depth shear resultant $T^d_{x\theta}$, along the diagonal, can be determined by considerations of global equilibrium along the global **Z** axis of a portion of the half web, identified by meridian angles 0 and θ_j and by the parallel angles 0 and $\pi/4$:

$$\sum_{i=1}^{m} (T^d_{x\theta} \cdot \sin \gamma_i) = -\rho \cdot t \cdot \int_0^{\underline{\theta_j}} R^2 \cdot \sin \underline{\theta} \cdot (\tan \pi/4 - \tan 0)\, d\underline{\theta} + S_j \cdot \sin \gamma_j =$$

$$= -\rho \cdot t \cdot R^2 \cdot \cos\left(1 - \cos \underline{\theta_j}\right) + S_j \cdot \sin \gamma_j \tag{23}$$

Hence, for a generic block i along the diagonal, identified by the surfaces j-1 and j, the shear force $T^d_{x\theta}$ is:

$$T^d_{x\theta} = \frac{-W_{tot} + S_j \cdot \sin \gamma_j - \sum_{i=1}^{m-1} (T^d_{x\theta} \cdot \sin \gamma_i)}{\sin \gamma_i} \tag{24}$$

The quantification of the shear stress resultant and its projection in the horizontal direction allows to calculate the parallel force H_p ($p = n$) along the diagonal:

$$H_n = T^d_{x\theta} \cdot \sin \alpha'_{k=\pi/4} \tag{25}$$

and, for horizontal equilibrium of a generic block the parallel force H_{p-1} is:

$$H_{p-1} = H_p - T_{\theta x\, j} + T_{\theta x\, j+1} - S_j \sin\alpha'_k + S_{j+1} \sin\alpha'_k - T_{x\theta\ p} \cdot \sin\alpha'_k + T_{x\theta\ p+1} \cdot \sin\alpha'_k \tag{26}$$

If H_p exceeds the tensile strength of the material (by assumption equal to zero), cracks can develop along the meridians and the hoop stresses are not present any more. Hence the horizontal equilibrium equation reduces to:

$$T_{\theta x\, j} + S_j \sin\alpha'_k + T_{x\theta\ p} \cdot \sin\alpha' = T_{\theta x\, j+1} + S_{j+1} \sin\alpha'_k + T_{x\theta\ p+1} \cdot \sin\alpha'_k \tag{27}$$

After cracking, also the shear force $T_{x\theta}$ can not be transmitted and hence, for equilibrium to rotation around an axis normal to the element surface (*z'* axis), also the resultant shear force $T_{\theta x}$ at the *j* interface and at the *j+1* interface are equal to zero.

Hence the meridian resultant S_j after cracking, indicated as S_j^*, only depends on the weight W_i and on the angles α_k and γ_j. The S_j^* can be calculated by means of a vectorial combination between W_i and S_{j-1} as follows:

$$S_j^* = \sqrt{\left(S_{j-1} \cos\alpha'_k \ \cos\gamma_j\right)^2 + \left(S_{j-1} \cos\alpha'_k \ \sin\gamma_j + W_i\right)^2} \tag{28}$$

And the corresponding angle γ^* is equal to:

$$\gamma_j^* = -\arctan \frac{S_{j-1} \sin\gamma_{j-1} + W_i}{S_{j-1} \cos\gamma_{j-1}} \tag{29}$$

In the cracked area, both the normal and shear resultant at the *j* interface of each block can be obtained as components of S^* as follows:

$$N_j = S^* \cdot \cos(\theta_j - \gamma_j^*) \tag{30}$$

$$T_j = S^* \cdot sen(\theta_j - \gamma_j^*) \tag{31}$$

Finally imposing the frictional constraint:

$$\sqrt{T_j^2 + T_{\theta x}^2} \le T_0 + N_j \mu \tag{32}$$

the optimum programming problem is completely defined if the maximum eccentricity of the thrust surface is minimized. It should be noted that T_j is the through depth shear resultant of stress, while, as discussed previously, $T_{\theta x}$ in (Equation 32) will be nonzero only in the uncracked area.

The eccentricity of the thrust surface at each point, that represents the target function to minimize, is:

$$e_j = \ \Delta R = \left|R_j^{geom} - R_j^t\right| \tag{33}$$

where the distance between the origin of the axes and each point of the thrust surface is:

$$R_j^t = \sqrt{\left(l_j^{geom}\right)^2 + \left(z_j^t\right)^2} = \sqrt{\left(\frac{x_j^{geom}}{\cos\alpha_k}\right)^2 + \left(z_j^t\right)^2} \tag{34}$$

and the distance between the origin of the axes and each point of the middle surface is:

$$R_j^{geom} = \sqrt{\left(\frac{x_j^{geom}}{\cos\alpha_k}\right)^2 + \left(z_j^{geom}\right)^2} \tag{35}$$

Hence, the minimum constant thickness t required is:

$$t_{\min} = 2\max \Delta R \tag{36}$$

Conditions in Equation (32) together with the target function in Equations (33) or (36) completely define the physical state of the vault and its mechanism of collapse, as the values of the indexes i and j for which the $=$ sign applied in Equations (32) and/or (33) identifies the cross sections along the arch for which either rotation or sliding are about to occur. Furthermore the resultant horizontal trust H^t_j is obtained by taking horizontal component of $S_j{}^*$ for each block in each slice. Of particular relevance is to identify where the value is maximum along the meridian, what is the value of it where the hinges form in the slice, and what is its distribution moving from the diagonal towards the centre of the web.

The static problem set in the terms outlined previously can be easily extended to generic conditions of loading and constraints because the symmetry is only invoked to define an initial value of shear resultant at midspan, but this definition can easily be obtained by using generic global equilibrium considerations. In the present treatment of the problem, the Coulomb condition is only invoked for the joints along the meridians. In reality, it should also be satisfied along the parallel joints where H_p is nonzero. This condition can be verified *a posteriori*.

3.3. Analysis of Results

In identifying the optimal thrust surface, the proposed analytical method, based on a lower bound approach, allows the quantification of important parameters for the safety assessment and strengthening requirements of pavilion vaults, such as:

- geometric safety factor, expressed as the ratio between the geometric thickness and the required minimum thickness (Equation 36) for a given load condition; if the ratio is >1, then the vault is safe;
- the hoop stress resultant (Equation 26) and hence the meridian crack pattern;
- the optimized thrust surface's eccentricity (Equation 33) and the hinge position;
- the optimized shear stress resultant at blocks interfaces (Equation 32) and sliding interface position, if any; and
- the horizontal thrust along the wall support.

To demonstrate the effectiveness of the procedure and to clarify the role of interaction between arches in complex vaults, the results are discussed below, presented in terms of meridian stress resultant S and its components N and T; thrust surface eccentricity e; value and distribution of the thrust at supports H_t.

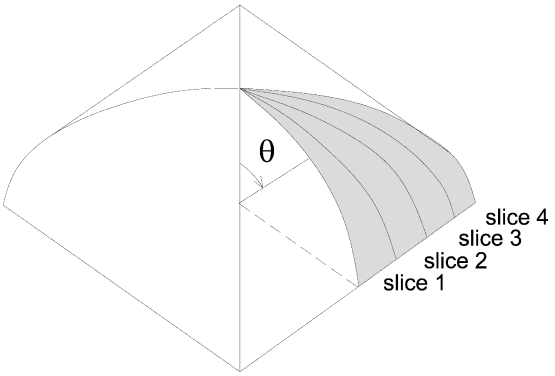

Figure 6. Schematic illustrations of the division of a half web in slices and nomenclature for the procedure.

The results are obtained by means of an electronic spreadsheet and a multipurpose mathematical programming, used to solve the problem of optimum. The commercial program Excel has been used. The Excel Solver allows setting the problems in terms of a target cell to be minimized by changing values in an array, whose values are dependent on other arrays limited by set constraints. A series of options can be chosen to control basic parameters, such as number of iterations and level of convergences, together with the type of algorithm used to determine estimates, derivatives and search directions for the next iteration. The Solver stops when a solution is found. The output also indicates whether the current solution is an optimum or simply a solution satisfying the set constraints. Tests performed using different choices of parameters, show that the target variables, in particular the resultants S^*, the horizontal forces H_p, and the horizontal thrust H_t, remain almost unchanged. Also the eccentricity, and hence the bending moment for all the slices, does not appear sensitive to these changes.

Considering a pavilion vault subjected to self-weight, with generatrix radius R equal to 3 m, vault rise f equal to 3m, span l equal to 6m and thickness t equal to 0.12m, the results are presented for four slices that comprise half of the web between the centre and the successive diagonal. Figure 6 shows the four slices that compose the portion of vaults considered. The web can be subdivided in a larger number of slices, as it is the case for the finite element mesh presented in section 4. This subdivision would reduce the difference in eccentricity's magnitude between slice 2 and 3 (Figure 10) as shown by the FE model results, but would not alter the trends of parameters and general behaviors identified by the limit state analysis. Specifically, for self-weight, there is no "singular" behavior within the web and hence no reason for further refinement of the mesh.

3.3.1. Meridian force S Wherever the hoop stress resultant assume tensile value, due the assumption of no tensile capacity, the meridian stress resultant is no more tangent to the meridian geometric curve and generally not centered. Figure 7 illustrates the variation of meridian resultant S with respect to the angle $\underline{\theta}$, in absence of cracking, after cracking has occurred and after cracking and optimization to obtain the minimum eccentricity, for slices 1 and 4. The diagrams show that the resultant S, before cracking, increases up to $\underline{\theta} = 45°$ for the central slice and up to $\underline{\theta} = 34°$ for the slice near to the diagonal, and reduces down to the support. This solution corresponds to the membrane solution that might occur if the material has the required tensile capacity. Since the masonry is generally not able

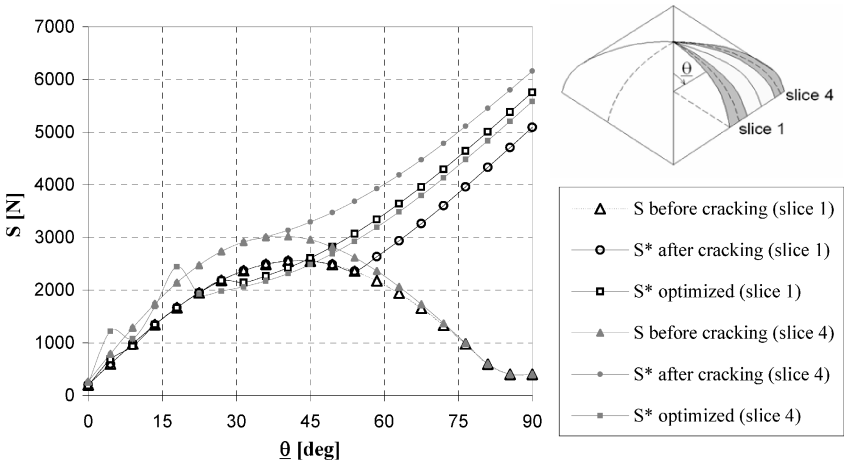

Figure 7. Graph of the meridian stress resultant S before cracking, after cracking and after the optimization for the central slice and for the slice near the diagonal.

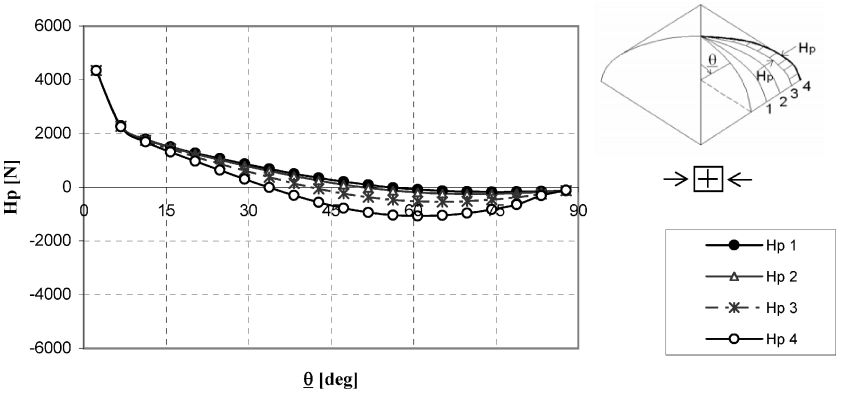

Figure 8. Graph of the hoop stress resultant along each slice, before cracking.

to resist tensile stresses, near the spring the cracks along the meridian direction will form and the force S^* departs from S along the cracked surface. In real cases cracks will appear initially in the weaker area and this is sufficient to counter the hoop strength along the corresponding parallels. In agreement with on-site observation, cracks in the model occur along the diagonals where, as it can be seen in Figure 8, hoop tensile stress resultants develop as from 34°. In the web the extension of cracking reduces and a maximum value of tensile stress H_p arise closer to the support (Figure 8).

Figure 7 also indicates the resultant S^* obtained minimizing the maximum thrust surface's eccentricity and imposing the material constrains. This force presents the same trend of the S^* before optimization, but the optimum S^* diverges earlier from the membrane solution, indicating that cracks will extend further towards the apex along the meridian. Furthermore, it emerges that the value of the S^* optimized is higher than S^* before optimization for the central slice, on the contrary it is smaller for the slice near the diagonal. This change in value is directly related to redistribution of stresses associated with the

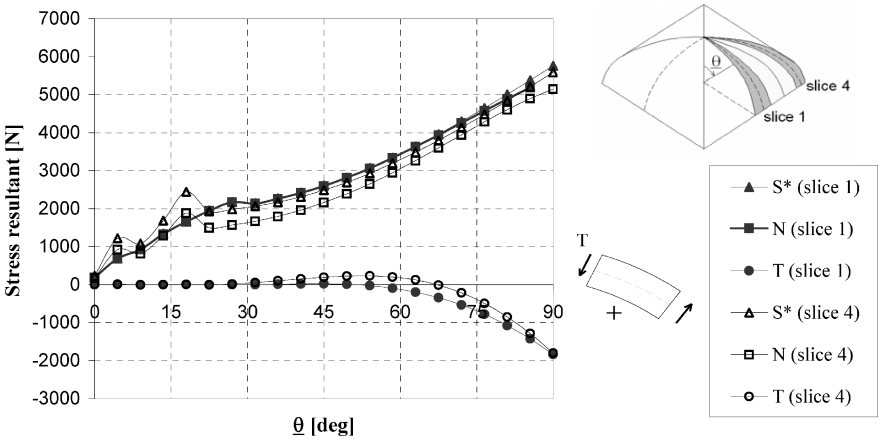

Figure 9. Graph of the resultant S^*, normal component N and parallel component T at the interface for the central slice and for the slice near the diagonal.

inclusion of the in depth shear in the equilibrium equations, which accounts for the 3D effects, and with the optimization of the eccentricity, especially for the slice closer to the diagonal as it will be seen in Figure 10.

3.3.2. Normal force N and shear force T at the interface The meridian normal stress resultant N and shear stress resultant T at the interface, components of S^* normal and parallel to the interface respectively, are shown in Figure 9. The resultant N reflects the same trend of S^* while the shear force T is equal to zero up to where the thrust line is perpendicular to the block interface, and it increases in the cracking area, where the funicular breaks away from the middle surface because of the absence of hoop stresses along the parallels. The negative value highlights that sliding will occur outwards, but for the diagonal, the region between 34 and 70 degrees has positive values, showing that if friction resistance were to lack, then the elements would move inward. Besides, it can be observed that, from the centre of the web to the diagonal, the shear force T increases only modestly, which will be reflected in a more uniform distribution of the thrust along the wall support.

3.3.3. Thrust surface eccentricity The thrust surface eccentricity is shown in Figure 10. It should be noted that, for slices 3 and 4, the non-optimized solution differs substantially from the optimum solution. The non optimized solution for all the slices, indeed, is equal to zero along the uncracked area and it has an exponential trend from the haunches to the support, because the absence of the hoop stresses requires an infinite thickness as the angle approaches 90°.

The eccentricity for the optimum solution, however, shows relative peaks indicating, for the slices 3 and 4, the formation of plastic hinges at the extrados, for θ_j of approximately 32°, and at the intrados, for θ_j of approximately 70°. Also for slices 1 and 2 the same trend applies, but the values are substantially lower and the relative maximum are at the extrados for θ_j of about 38° and at the intrados for θ_j of approximately 55°. At the support the eccentricity after optimization is greater for the central slices than for the ones approaching

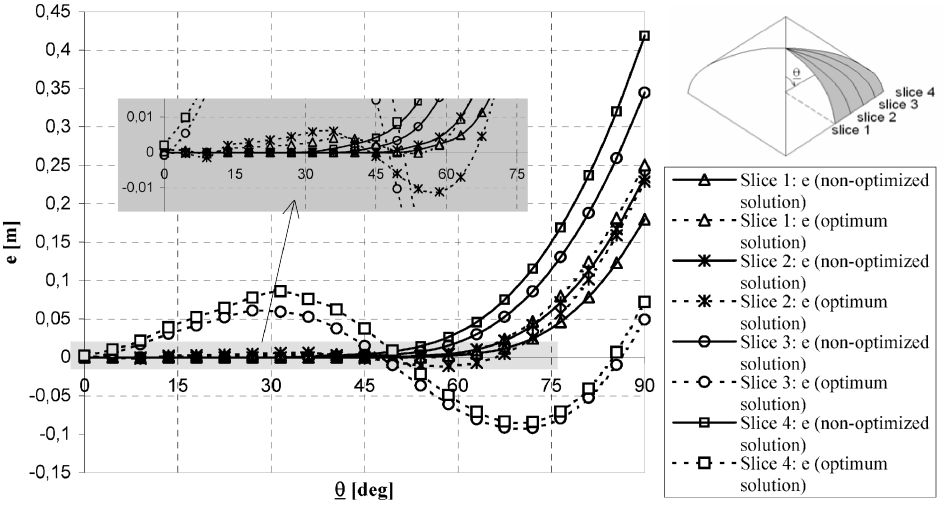

Figure 10. Graph of the thrust surface eccentricity for the nonoptimized solution and for the optimum solution (slice near to diagonal).

the diagonal. However, the presence of abutment walls in this area usually is sufficient to guarantee equilibrium.

As stated earlier, the load condition considered is equivalent to self-weight. This is calculated with respect to a reference initial thickness and hence should be considered as a nominal load distribution akin to self-weight. Any uniformly additional gravitational load imposed over the vault by cladding or snow, would be a proportion of this and hence to minimize the thickness represent the inverse problem of maximizing the load, or, in other words, defining the efficiency of the vault.

The diagram in Figure 11 shows the corresponding bending moment for the four slices, calculated as the product of the meridian normal resultant N_{jk} and the eccentricity e_{jk}. As it can be seen, the maximum bending moment for all slices is localized at the

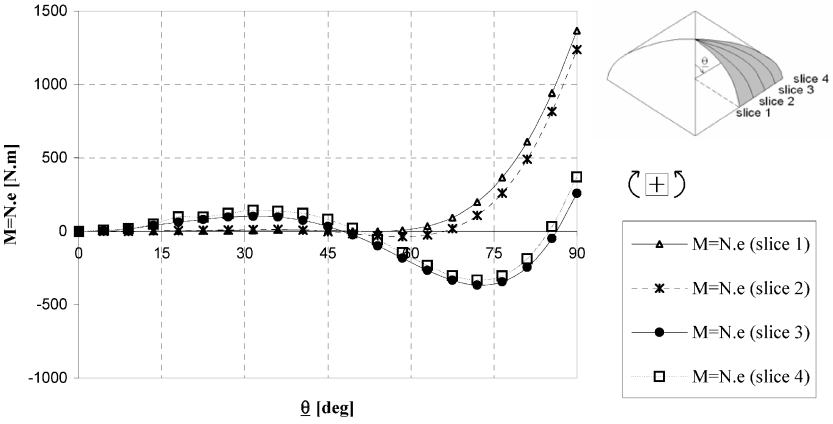

Figure 11. Graph of the bending moment for all the slices belonging to half web.

support confirming the presence of extrados plastic hinges there or parallel cracks. However the position of the other two relative maxima on slices 4 and 3 means that the collapse mechanism will not be contained in a vertical plane, and hence the necessity of a full 3D analysis

3.3.4. Horizontal thrust at the supports The possible intrados plastic hinges at $\theta_j = 70°$ for slices 3 and 4 and at $\theta_j = 55°$ for slices 1 and 2, and the presence of the spandrel, that contributes to increase the thickness in the portion of the vault nearer the support, entails that the horizontal thrust is best evaluated at $= 70°$ for the slices 3 and 4 and at $\theta_j = 55°$ for the slices 1 and 2. Furthermore, as it can be seen in Figure 12, showing the horizontal component of S^* along the meridian for the 4 slices, H_t is constant in the cracked area, where hoop stresses are nil.

For the horizontal thrust evaluation, it is also necessary to consider that the stiffness of the perimeter walls influences the horizontal thrust: the maximum horizontal thrust corresponds to thick walls, in the limit comparable to a hinge, and minimum horizontal thrust corresponds to thin flexible walls, in the limit assumed as roller. In the present analysis the wall support condition corresponds to a hinge. Minimizing the eccentricity, also minimizes the angle γ_j, i.e. the inclination of S on the horizontal, and hence maximizes its horizontal component H_t. This means that it is indeed both necessary and sufficient to minimize the eccentricity to obtain the correct hinges' position and the corresponding maximum horizontal thrust. The quantification and position of horizontal thrust is very important in strengthening interventions because it allows to determine the ties required capacity and their appropriate location along the meridian.

Figure 13 shows the distribution of the thrust along a parallel, for the non-optimum solution and for the solution after optimization. Because all slices present the same rise but increasing span from the centre to the diagonal, in the nonoptimized solution, which does not takes into account lateral redistribution, the minimum thrust is localized at the centre of the web, where the slice's rise to span ratio is highest. Instead, the optimum

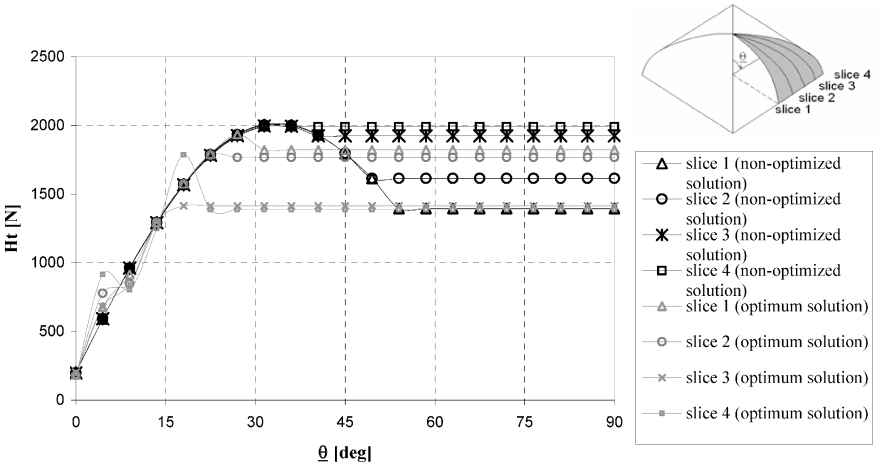

Figure 12. Graph of the horizontal thrust H_t along the meridian before and after optimization.

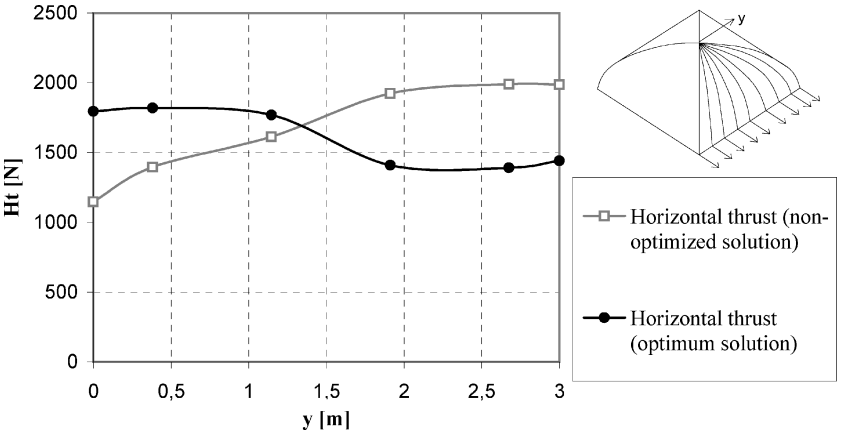

Figure 13. Graph of the horizontal thrust for the non-optimum solution and for the solution after the optimization.

solution exhibits a trend with a maximum on the first slice, and then decreasing towards the diagonal. This means that natural lateral arches in the web will develop.

3.4. Remarks on Structural Behavior of Pavilion Vaults

The procedure presented in the previous sections allows clarification of some important aspects of the complex structural behavior of pavilion vaults, in particular concerning the 3D effects and the importance of sliding failure. The results demonstrate that the cracking along the diagonal is independent of the support stiffness (Figure 8), unlike the common opinion that consider the diagonal cracks a consequence of the supporting walls' overturning at the corner. The results presented above also demonstrate that, despite the cracks along the diagonals, within each web arches can transfers stresses to adjacent ones, through shear action, and hence the lateral continuity cannot be ignored. This interaction is clear observing the distribution of horizontal thrust along the support (Figure 13): as it can be seen, the horizontal thrust in the limit analysis solution (Figure 14c) has a more even distribution, and it is independent of the modeling of the simplified arches (Figure 14a; 14b) contrary to what is usually proposed in literature (Cangi 2005).

The complex crack pattern and collapse mechanism that develops, according to the limit state analysis approach, is represented in Figure 15. The more extensive cracking occurring in the diagonal region implies that the lateral slices will tend to behave almost as independent arches, This results in the thrust line having greater eccentricity and hence in plastic hinges forming, the first at the extrados, for $\overline{\theta_j}$ equal to 32° on the 4th slice, the second at the intrados, for $\overline{\theta_j}$ equal to 70° on the 3rd slice. The central region, cracked only in the lower portion, still exhibits shell behavior and the thrust surface here deflects from the mean surface of the vault only in the region close to the support, with high inclination of the stress resultant so that both the thrust and through depth shear stress resultant are maximum and the third hinge forms in the 1st slice for $\overline{\theta_j}$ equal to 90°.

Moreover considering variable values of friction, Figure 16 shows that, for friction coefficient higher than 0.50, the shear force T are everywhere smaller than $N.\mu$, hence the results are unrelated to the friction coefficient and sliding mechanism are prevented.

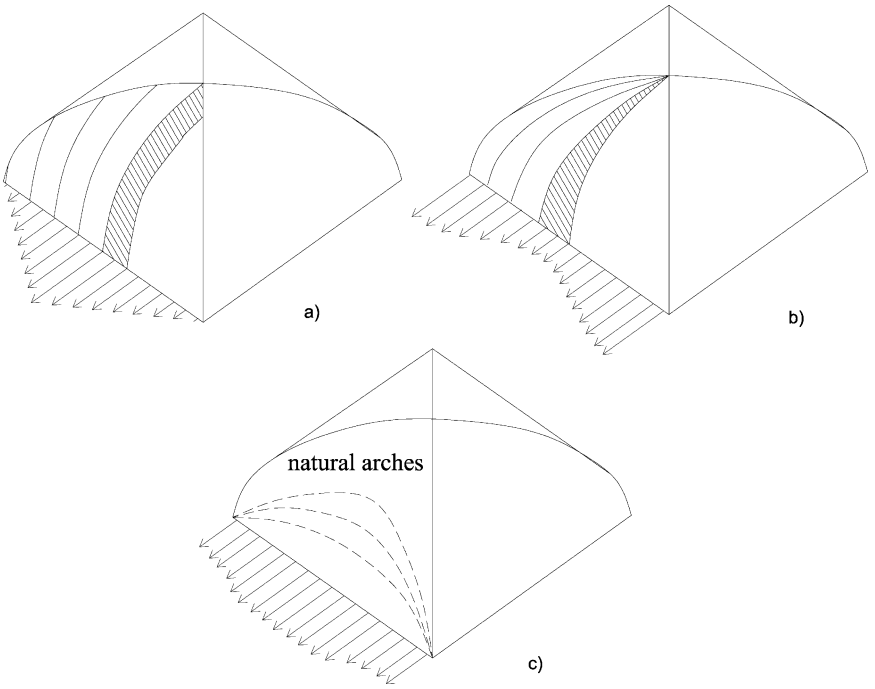

Figure 14. Schematic illustrations of the horizontal thrust along the supports obtained by the simplified arch model with (a) parallel arches and with (b) slices, and (c) horizontal thrust obtained by the limit state analysis.

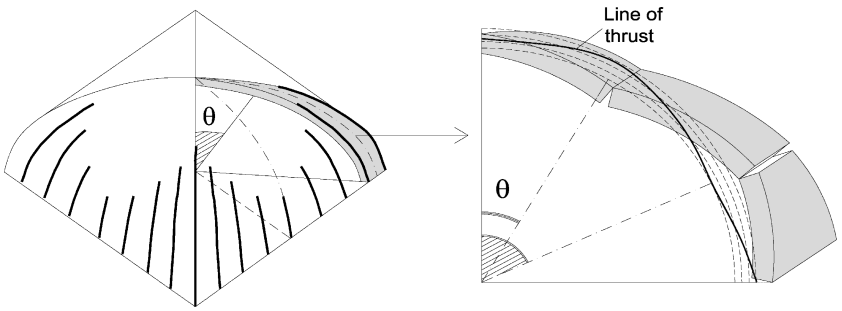

Figure 15. Schematic illustrations of the possible vault's collapse mechanism for the slice next to the diagonal.

In contrast, in the friction coefficient range of 0.3-0.50, the vault is able to find a new equilibrium system, in which the stress resultants are unvaried, but the eccentricity considerably increases (Figure 16). This means that the thickness necessary for the vault's stability would increase and consequently the geometric safety factor decrease. However as seen from Figure 10, the maximum eccentricity computed by the procedure is located at the support, where typically the spandrel ensures a larger available thickness. If the blocks are not confined, sliding could occur at this level and this would facilitate the development of the hinge mechanism as shown in Figure 15. This range of solutions is of particular interest as Vasconcelos and Lourenço (2006) report value of friction coefficient for historic

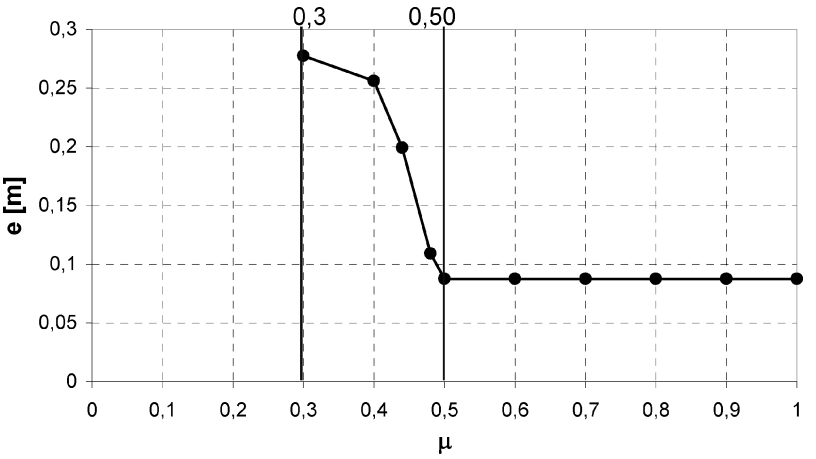

Figure 16. Graph of the maximum thrust surface eccentricity obtained with the limit state analysis with finite friction for different friction coefficients μ.

masonry lower than 0.4. For friction coefficients lower than 0.3 the Excel's solver cannot find a feasible solution, i.e. it cannot satisfy all constraints.

4. VALIDATION OF THE PROCEDURE: COMPARISON WITH FINITE ELEMENT MODEL (FEM)

The validation of the proposed procedure is carried out by comparing the results in terms of stress resultants with the output obtained by advanced nonlinear FEM. The FEM has been constructed using the *Algor V21* FE program, released by Algor, Inc., and the modeling option chosen is the *mechanical event simulation with nonlinear material model*.

The vault has been modeled using four-node nonlinear shell elements for all uncracked masonry portions. For the shell elements, the material "curve with isotropic hardening" and the constitutive laws reported in Figure 17 have been adopted, with the following mechanical properties for the masonry: density γ=1850 kg/m^3; Poisson's ratio ν=0.15; elastic modulus E=5000 MPa.

With an iterative procedure, the regions subjected to tensile stresses are localized and nonlinear contact elements are placed at the interface between shell elements (Figure 18a).

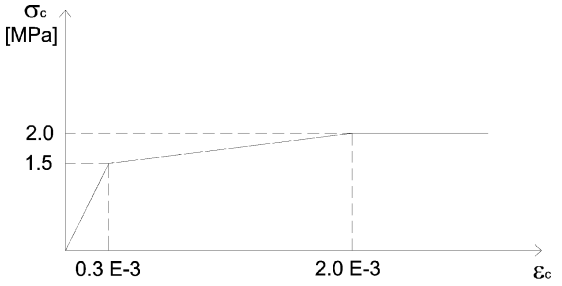

Figure 17. Constitutive law for shell elements representing uncracked masonry (valid for compression only).

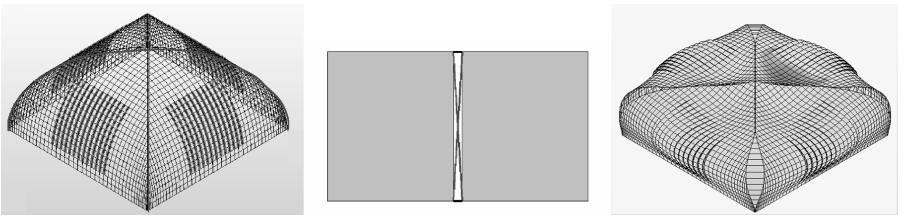

Figure 18. Schematic illustrations of (a) the positioning of contact elements, (b) detail of diagonal contact elements, and (c) axonometric view showing the finite elements model of pavilion vault.

In order to simulate the shear strength associated to friction, when contact is active, diagonal contact elements are also added (Figure 18b). For the contact elements the unlocked tension modulus adopted is 0.0 N/m^2 and the unlocked and locked compression modulus is 5000 MPa for the horizontal and diagonal. Cross sections of the elements are calibrated to obtain same deformation and equivalent stress resultants at the shell's node when the contact elements are active.

For an easier comparison between the results of the limit state analysis and the FE analysis, the FE mesh has half the size of the limit state analysis along the parallel but the same number of subdivisions along the meridian. Hence, as it can be seen in Figure 18c, the web between the center and the successive diagonal comprises 8 slices and 20 parallels. To simulate the presence of perimeter walls 3 m high and 0.50 m thick, shell elements are added along the supports and constrained not to translate in the three global directions.

Figure19 shows the comparison between the meridian stress resultant *S* obtained with the optimized limit state analysis and with FEM along the central slice and along the slice near to the diagonal, respectively. Results show good agreement, both in terms of values of the stress resultants and identification of the cracked portion. Moreover, in agreement with the safety theorem of limit state analysis associated with lower bound approaches, the values of *S* as calculated by the limit state procedure are always slightly greater than the state of stress identified by the FE analysis. Modest numerical instability is present in both models due to the nature of the simulation in both cases.

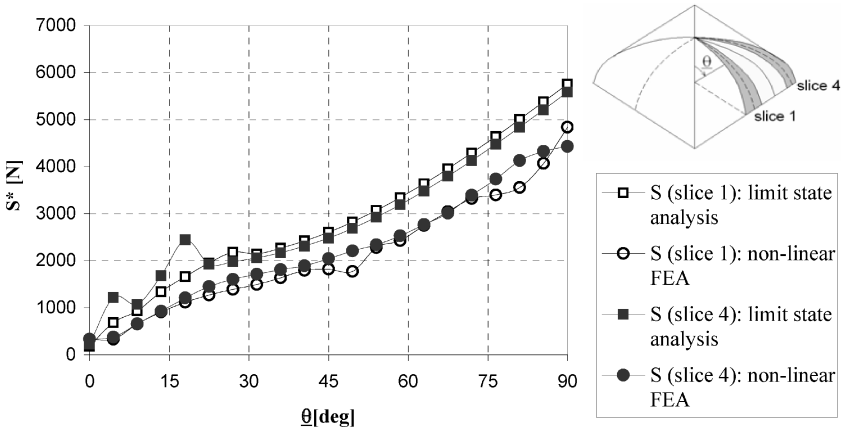

Figure 19. Graph of the comparison between the meridian forces S obtained by the limit state analysis and by the finite elements analysis along the central slice and along the slice near the diagonal.

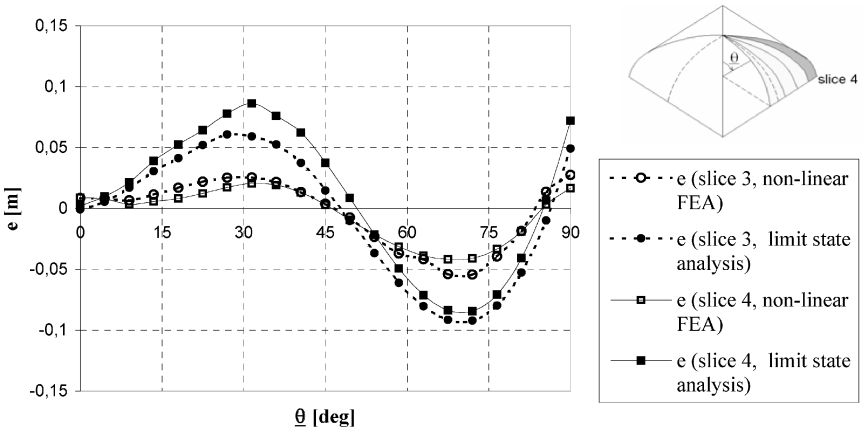

Figure 20. Graph of the comparison between the eccentricities obtained by the limit state analysis and by the finite elements analysis along the slice near the diagonal.

The normal stress resultant N and shear stress resultant T also show the same level of accuracy, implying that also the angle γ and hence the direction of S and the inclination of the line of trust are properly computed. As it can be seen in Figure 20, in favor of safety, the values of eccentricity computed by the procedure are greater than the values obtained with the FE, however the location of relative minimum and maximum and absolute values identify with great accuracy the position of plastic hinges along the slices. The difference in value of the eccentricity might be ascribed to the difference in stiffness at the support.

The identification of the position of the intrados hinge is particularly critical, as this also defines the position along the arch of the maximum horizontal thrust and hence it is essential for the correct positioning of ties or for the construction of abutments.

Values of horizontal thrust have been compared for the two analyses for an angle θ=65° and for the condition of full lateral restraint at the support for the F.E. model.

As shown in Figure 21, where the thrust is plotted along a half parallel between midspan (y=0) and the diagonal, the trend is similar in the two cases with the values estimated by the procedure being clearly equal to the F.E at midspan and slightly overestimated as progresses toward the diagonal with a maximum difference of 10%.

5. CASE OF STUDY OF ST. PIER D'AGRINO CHURCH IN GARGNANO, ITALY

Finally the procedure is applied to the assessment of a real case pavilion vault to verify whether location and extension of estimated cracks are correct. The St. Pier D'Agrino church in Gargnano (Brescia, Italy) (Figure 22) is a late Renaissance building, with a nave and the two aisles, separated by Doric columns, built in the 1576. Four chapels were added in 1580. In the 17th century, a choir was built and the presbytery was enlarged and heightened assuming a square plan. The presbytery was covered with a shallow pavilion vault with a 6.2 m span, a 2 m rise and a 0.25 m constant thickness (Figure 23). The generatrix at the center of the web is a circular arc of radius R= 3.1m and subtending angle θ =65. As shown in Figure 24, the vault is affected by cracks along the four diagonals of different width and extension.

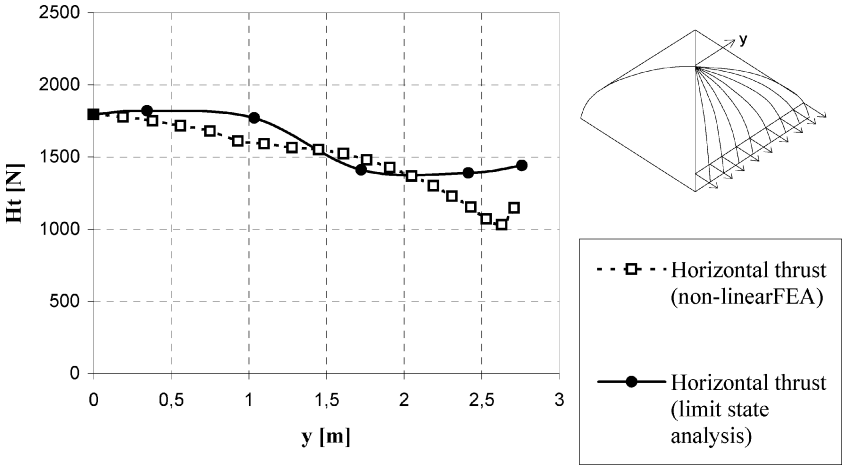

Figure 21. Graph of the comparison between the horizontal thrust obtained by the limit state analysis and by the Finite Elements Analysis.

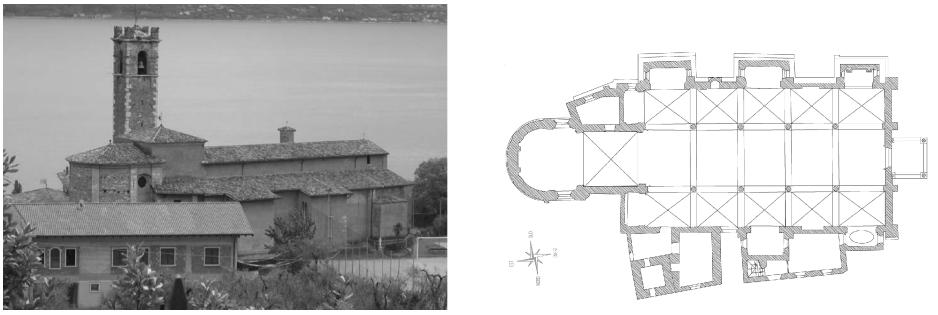

Figure 22. Photograph (left) and plan (right) of St. Pier D'Agrino church (Brescia, Italy).

Figure 23. Photograph of the intrados view of the presbytery's pavilion vault.

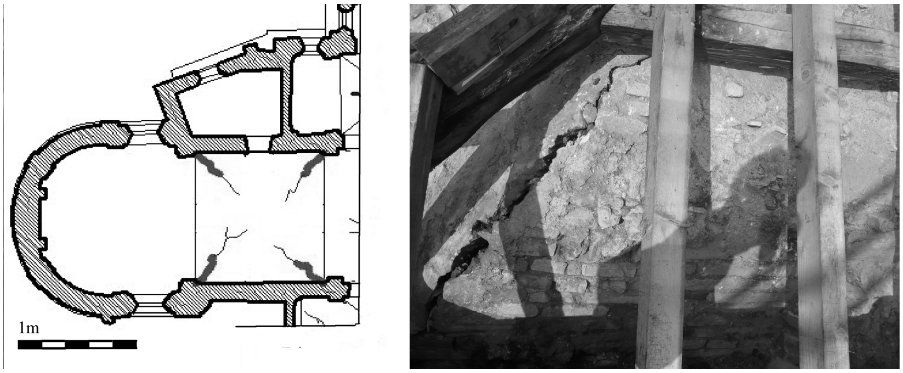

Figure 24. Schematic illustration of the crack pattern of the presbytery's pavilion vault of S. Pier d'Agrino church (left) and photograph of the crack along a diagonal from extrados (right).

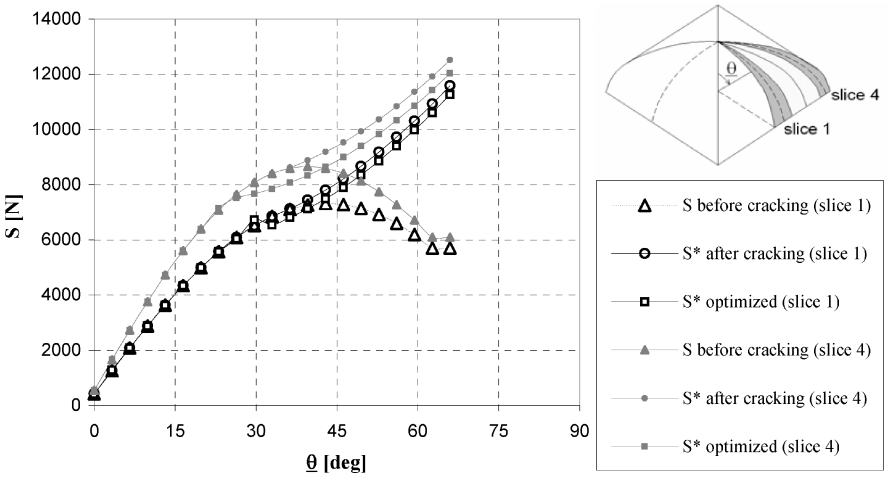

Figure 25. Graph of the meridian force S before cracking, after cracking and after the optimization for the central slice and for the slice near the diagonal of pavilion vault in the St. Pier D'Agrino church.

Using the same notation and the same division in slices previously described, Figure 25 shows the meridian stress resultant S obtained for the central slice and for the slice near the diagonal. It can be noted that the extension of the meridian cracking is reduced with respect to the circular profile generatrix analyzed in the previous section. Indeed, as it is demonstrated by D'Ayala and Tomasoni (2008), decreasing the rise to span ratio, the classical membrane solution, that represents the stress field before meridian cracking, is closer to the optimum solution. This implies that the length of the crack developing along the diagonal increases with the vault's rise. Conversely the compression hoop stresses H_p, before optimization show exactly the same distribution as the circular case, except for the element adjacent to the support (Figure 26). Given the profile of the vault and the observation above, it also follows that the shear stress resultant has modest values, and that the eccentricity after optimization is substantially reduced, with a maximum

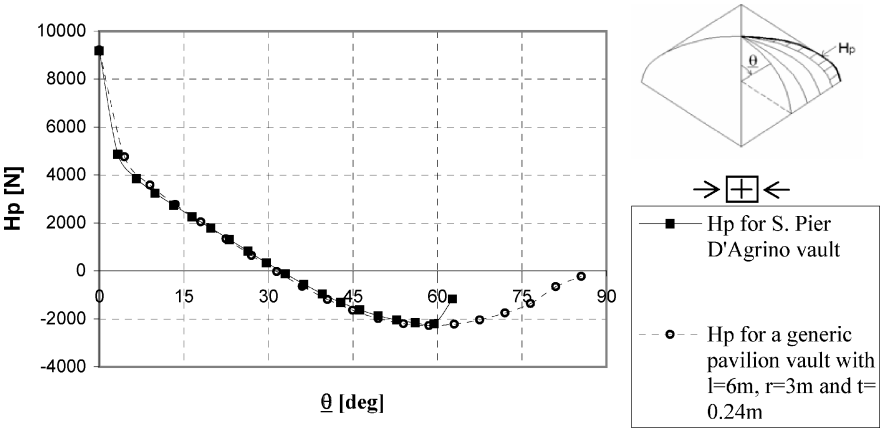

Figure 26. Graph of the comparison between the hoop stresses H_p obtained by the limit state analysis for the St. Pier d'Agrino vault (rise-span ratio approximately equal to one-third) and the generic pavilion vault with a rise-span ratio equal to one-half.

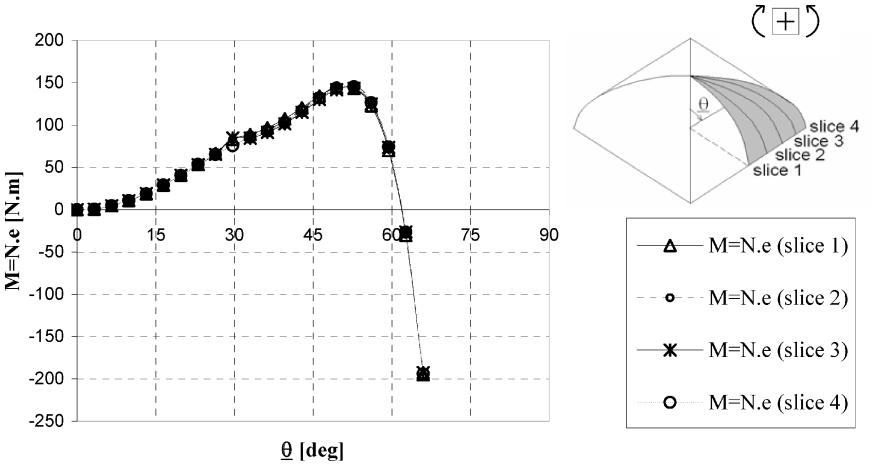

Figure 27. Graph of the bending moment for all the slices belonging to half web.

intrados value of 0.018 m for θ=55 The modest value of eccentricity is confirmed by the absence of parallel cracks at the extrados of the vault near the haunches.

Finally, resultant meridian moment and horizontal thrust are plotted in Figure 27 and 28. In the case study as expected the horizontal thrust at the supports (rise-span ratio approximately equal to one-third) is greater than the horizontal thrust in a pavilion vault with the same thickness but a rise-span ratio equal to one-half. Furthermore is possible to observe that its trend along the perimeter walls tends to become constant for shallower vaults. This means that, reducing the rise/span ratio, both the value of S^* and the angle γ^* at the haunches remains about constant along the perimeter wall.

D'AgrinoD'Agrinod'Agrino

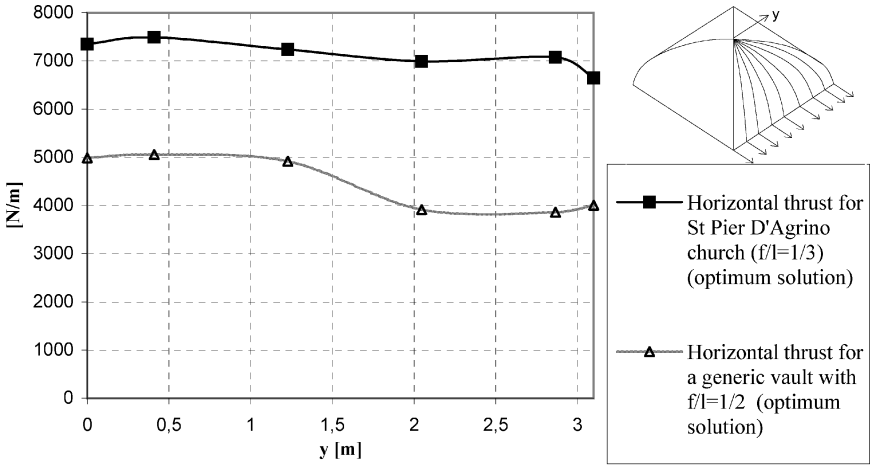

Figure 28. Graph of the comparison between horizontal thrust along the supports for the St. Pier d'Agrino vault (rise-span ratio approximately equal to one-third) and for a generic pavilion vault with the same thickness but a rise-span ratio equal to one-half.

6. CONCLUSIONS

The present article proposes a procedure for 3D analysis of vaulted structures based on limit state analysis under the assumption of finite friction. This approach enables to describe the structural behavior of a wide range of masonry vaults, including masonry complex vaults, for instance pavilion vaults, fan vaults and cross vaults.

Starting from an initial surface of thrust, corresponding to median surface of the vault, and assuming finite friction between blocks' interfaces, the procedure computes the position of the optimal thrust surface. Furthermore, this approach is able to provide in very modest time (by use of electronic spreadsheets and commercially available multipurpose Solver routines) results in good agreement with the ones obtained by means of nonlinear FEA analysis, often too laborious because of their high computational burden and the difficulty in interpretation of the results. As it is demonstrated in the present paper, the crack pattern, the stress resultant and horizontal thrust are accurately predicted by the proposed procedure. This means that limit state analysis with finite friction allows to identify all the important elements in a strengthening intervention, as well as the geometric safety factor of the vault, given by the actual thickness over the minimum thickness ratio.

Furthermore limit state analysis with finite friction allows investigating two aspects previously neglected for masonry vaults: the possibility of sliding mechanisms between the blocks and the importance of three-dimensional stress fields in the equilibrium of complex vaults. Particularly the analysis has been able to show that for values of the coefficient of friction smaller than 0.5, sliding becomes a critical failure mode and further increases in thickness are necessary to re-establish equilibrium. Given that typical historic masonry has values of friction of the order of 0.4–0.6, and given the difficulty of reliably assessing the shear capacity, the procedure shows that checks against sliding are critical and more relevant as the rise to span ratio increases.

The application to pavilion vaults has shown that also vaults with rigid boundary at the supports are affected by cracks along the diagonals, unlike the common opinion that

ascribes the diagonal cracks only to the walls overturning and that the actual horizontal thrust is about constant along the perimeter, with greater values at the centre for higher rise to span ratios.

ACKNOWLEDGEMENT

The authors wish to thank Prof. Ezio Giuriani from the University of Brescia for suggesting the topic and providing critical insight during the development of this study and arch. Mauro Biasin for access to the material on S. Pier D'Agrino church.

REFERENCES

Amadei, B., C. T. Ling, B. Shing, B., G. Mirabella, G., and L. Binda. 1995. Modelling the stability of masonry structures with the discontinuous deformation analysis (DDA) method. In *Proceedings of the 3rd International Symposium Computer Methods in Structural Masonry*, April 19–21, 1995, Lisbon, eds., J. Middleton and G. Pande. Swansea, UK: Books & Journals International.

Andreu, A., L. Gil, and P. Roca. 2007. Computational analysis of masonry structures with a funicular model. *Journal of Engineering Mechanics, ASCE* 133(4):373–480.

Atkinson, R. H., B. P. Amadei, S. Saeb, S., and S. Sture. 1989. Response of masonry bed joints in direct shear. *Journal of Structural Engineering, ASCE* 115(9):2276–96.

Baggio, C., and P. Trovalusci. 1998. Limit analysis for no-tension and frictional three-dimensional discrete systems. *Mechanics of Structures and Machines* 26(3):287–304.

Block, P., and J. Ochsendorf. 2008. Lower-bound analysis of masonry vaults. In *Proceedings of the 6th International Conference Structural Analysis of Historical Construction*, July 2–4, 2008, Bath, eds., D. F. D'Ayala and Fodde. London, UK: Taylor & Francis Group.

Boothby, T. E. 1994. Stability of masonry piers and arches including sliding. *Journal of Engineering Mechanics* 120(2):304–319.

Breymann, G. A. 2003. *Archi, volte, cupole (1885)*. Rome, Italy: Dedalo.

Calderini, C., and S. Lagomarsino. 2006. A micromechanical inelastic model for historical masonry. *Journal of Earthquake Engineering* 10(4):453–479.

Cangi, G. 2005. *Manuale del recupero strutturale e antisismico*. Rome, Italy: DEI.

Cattari, S., S. Resemini, and S. Lagomarsino. 2008. Modelling of vaults as equivalent diaphragms in 3D seismic analysis of masonry buildings. In *Proceedings of the 6th International Conference Structural Analysis of Historical Construction*, July 2–4, 2008, Bath, eds., D. F. D'Ayala and Fodde. London, UK: Taylor & Francis Group.

Cundall, A. 1971. Formulation of three-dimensional distinct element model-part I: a scheme to detect and represent contacts in a system composed of masonry polyhedral blocks. *International Journal of Rock Mechanics and Mining Sciences and Geomechanics* 25(3):107–116.

Curioni, G. 1870. *L'arte di fabbricare. Costruzioni civili, stradali, idrauliche*. Torino, Italy: Negro.

D'Ayala, D. 1993. Analytical method for the assessment of the safety levels of domes. In *Proceedings of the 3rd International Conference Structural Studies, Repairs and Maintenance of Historical Buildings (STREMAH)*, June 16–18, Bath, eds., C. Brebbia and R. Frewer. Southampton, UK: Computational Mechanics Publications.

D'Ayala, D. 1994. *In tema di comportamento strutturale delle cupole in muratura*. University "La Sapienza" Doctoral Thesis, Rome, Italy.

D'Ayala, D., and C. Casapulla. 2001. Limit state analysis of hemispherical domes with finite friction. In *Proceedings of the 3rd International Conference Structural Analysis of Historical Constructions*, November 7–9, 2001, eds., P. Lourenço and P. Roca. Guimaraes, Portugal: Balkema.

D'Ayala, D., and E. Tomasoni. 2008. Study on structural behaviour of masonry vaults: limit state analysis with finite friction. In *Proceedings of the 6th International Conference Structural Analysis of Historical Construction*, July 2–4, 2008, Bath, eds., eds., D. F. D'Ayala and Fodde. London, UK: Taylor & Francis Group.

De Josselin de Jong, G. 1964. Lower bound collapse theorem and lack of normality of strain rate to yield surface for soils. In *Proceedings of the I.U.T.A.M. symposium Rheology and soil mechanics*, 1964, Grenoble. West Berlin, Germany: Springer-Verlag.

Drucker, D. C. 1954. Coulomb friction, plasticity and limit load. *Journal of Applied Mechanics* 21(1):71–74.

Ferris, M. C., and F. Tin-Loi. 2001. Limit analysis of frictional block assemblies as a mathematical program with complementarity constraints. *International Journal of Mechanical Sciences* 43(1):209–224.

Flügge, W. 1973. *Stresses in shells*. Berlin, Germany: Springer & Verlag.

Gilbert, M., and C. Melbourne. 1994. Rigid-block analysis of masonry structures. *Structural Engineer* 72(21):356–361.

Harvey, W. J. 1988. Application of the mechanism analysis to masonry arches. *Structural Engineer* 66(5):77–84.

Heyman, J. 1966. The stone skeleton. *International Journal of Solids and Structures* 2: 249–279.

Heyman, J. 1977. *Equilibrium of shell structures*. Oxford, UK: Clarendon Press.

Huerta, S. 2001. Mechanics of masonry vaults: The equilibrium approach. In *Proceedings of the 3rd International Conference Structural Analysis of Historical Constructions*, November 7–9, 2001, Guimaraes, Portugal, eds., P. Lourenço and P. Roca. Guimaraes, Portugal: Balkema.

Lemos, J. V. 1997. Discrete element modelling of the seismic behavior of stone masonry arches. In *Proceedings of the 4th International Symposium Computer Methods in Structural Masonry*, September, 1997, Florence, eds., J. Middleton and G. Pande. Swansea, UK: Books & Journals International.

Levi, C. 1932. *Trattato teorico-pratico di costruzioni civili, rurali, stradali ed idrauliche*. Milan, Italy: Hoepli.

Livesley, R. K. 1978. Limit analysis of structures formed from rigid blocks. *International Journal for Numerical Methods in Engineering* 12(12):1853–1871.

Livesley, R. K. 1992. A computational model for the limit analysis of three-dimensional masonry structures. *Meccanica* 27(3):161–172.

Lourenço, P. B. 1996. *Computational strategies for masonry structures*. Delft University of Technology Doctoral Thesis. Delft: University Press.

Lourenço, P. B., and J. G. Rots. 1997. A multi-surface interface model for the analysis of masonry structures. *Journal of Engineering Mechanics, ASCE* 123(7):660–668.

Lourenço, P. B. 2001. Analysis of historical constructions: From thrust-lines to advanced simulations Historical Constructions. In *Proceedings of the 3rd International Conference Structural Analysis of Historical Constructions*, November 7–9, 2001, eds., P. Lourenço and P. Roca. Guimaraes, Portugal: Balkema.

Lourenço, P. B. and L. F. Ramos. 2004. Characterization of cyclic behavior of dry masonry joint. *Journal of Structural Engineering, ASCE* 130(5):779–786.

Magenes, G. 1992. *Seismic behavior of brick masonry: strength and failure mechanisms*. University of Pavia Doctoral Thesis. Pavia, Italy.

Michalowski, R., and Z. Mróz. 1978. Associated and non-associated sliding rules in contact friction problems. *Archives of Mechanics* 30: 259–276.

Mirabella Roberti, G., L. Binda, and G. Cardani. 1997. Numerical modeling of shear bond tests on small brick-masonry assemblages. In *Proceedings of the 4th International Symposium Computer Methods in Structural Masonry*, September, 1997, Florence, eds., J. Middleton and G. Pande. Swansea, UK: Books & Journals International.

Mirabella R. G., and F. Calvetti. 1998. Distinct element analysis of stone arches. In *Proceedings of the second international conference on arches and bridges*, October 6–9, 1998, Venice, ed., A. Sinopoli. Rotterdam, The Netherlands: Balkema.

O'Dwyer, D. 1999. Funicular analysis of masonry vaults. *Computer and Structures* 73(1–5):187–197.

Oppenheim, I. J., D. J. Gunaratnam, and R. H. Allen. 1989. Limit state analysis of masonry domes. *Journal of Structural Engineering, ASCE*. 115(4):868–882.

Orduna, A., and P. Lourenço. 2005a. Three-dimensional limit analysis of rigid blocks assemblages. Part I: Torsion failure on frictional interfaces and limit analysis formulation. *International Journal of Solids and Structures* 42(18):5140–5160.

Orduna, A., and P. Lourenço. 2005b. Three-dimensional limit analysis of rigid blocks assemblages. Part II: Load-path following solution procedure and validation. *International Journal of Solids and Structures* 42(19):5161–5180.

Palmer, A. C. 1966. A limit theorem for materials with non associated flow laws. *Journal de Mécanique* 5(2):217–222.

Scamozzi, V. 1964. *L'idea dell'architettura universale (1615)*, Ridgewood,.

Smars, P. 2000. *Etudes sur la stabilité des arcs et voûtes*. Katholieke Universiteit Leuven Doctoral Thesis. Leuven, Belgium.

Smars, P. 2008. Influence of friction and tensile resistance on the stability of masonry arches. In *Proceedings of the 6th International Conference Structural Analysis of Historical Construction*, July 2–4, 2008, Bath, eds., D. F. D'Ayala and Fodde. London, UK: Taylor & Francis Group.

Tomasoni, E. 2008. *Le volte in muratura negli edifici storici: Tecniche costruttive e comportamento strutturale*. Rome, Italy: Aracne Editrice.

Vasconcelos. G., and P. B. Lourenço. 2006. Assessment of the in-plane shear strength of stone masonry walls by simplified models. In *Proceedings of the 5th International Conference Structural Analysis of Historical Construction*, November 6–8, 2006, New Delhi, India, eds., P. Lourenço, P. Roca, C. Modena, and S. Agrawal. New Delhi, India: Macmillan India, Ltd.

APPENDIX

Notation: In order to facilitate the readability of this article, the symbols used in the theoretical formulation are defined in the following (Figure 1 and Figure 2):

NOTATION

α_k	angle between the x global axis and the projection of the generatrix on the horizontal plane
α_p	Horizontal angle between x axis in the global system and projection of lateral surface of a generic block in the horizontal plane
α'_k	Projection in the plane tangent to the thrust surface of angle α_k
γ_i	Angle between tangent of the thrust line and horizontal axis at the centre of the element (or angle between perpendicular to thrust line and vertical in the x'z' plane)
γ_j	Angle between tangent of the thrust line and horizontal axis at the block interface
γ^*_j	Angle between γ_j after cracking
$\underline{\gamma_j}$	Angle between perpendicular to thrust line and vertical in the XZ plane
$\underline{\gamma_{jLim}}$	Limiting value of angle γ_j
θ_j, θ_i	Angle between vertical and perpendicular to the element's surface at the centre of the element and at the block interface

θ_{i}	Angle between the vertical and perpendicular to the generatrix
ϕ	Angle of friction
μ	Coefficient of friction (tan ϕ)
ρ	Weight for unit volume
$\boldsymbol{E}$	Extrados surface
$\mathrm{e_j}$	Eccentricity of the thrust surface with respect of the median surface at the point of application of S_j
f	Vault rise
$\mathrm{H_p}$, $\mathrm{H_{p+1}}$	Hoop stresses
$\mathrm{H_{tj}}$	Resultant horizontal trust
$\boldsymbol{I}$	Intrados surface
l	Vault span
$\mathrm{l}_i^{geom} = \mathrm{l}_i^t$	Horizontal projection of the distance between the block's centre of mass and the origin of the global system
$\mathrm{l}_j^t = \mathrm{l}_j^{geom}$	Horizontal projection of the distance between the interface and the origin of the global system
m	Number of blocks in a slices
$\mathrm{N_j}$	Compressive force resultant, component of $\mathrm{S_j}$ normal to the interface
$\mathrm{N_{Lim}}$	Limiting value of $\mathrm{N_j}$
n	Number of slices
R	Constant radius of the generatrix
$\mathrm{R}_i^t = \mathrm{R}_j^t$	Distance of the trust surface from the origin of the coordinate
$\mathrm{R}_i^{geom} = \mathrm{R}_j^{geom}$	Distance of the median shell surface from the origin of the coordinate
$\mathrm{S_j}$	Meridian resultant of stress at interface j
$\mathrm{S_{Lim}}$	Limiting value of $\mathrm{S_j}$
S^*	Meridian resultant after cracking
T	Thrust surface
$\mathrm{T_j}$	Shear force resultant, component of $\mathrm{S_j}$ parallel to the interface
$\mathrm{T_{Lim}}$	Limiting value of $\mathrm{T_j}$
$\mathrm{T_0}$	finite cohesion
$\mathrm{T_{x\theta p}}$	In plane shear force at meridian interfaces
$\mathrm{T_{x\theta j}}$	In plane shear force at parallel interfaces
$T_{x\theta}^d$	Shear force along the diagonal
$\mathrm{t_{min}}$	Minimum constant thickness required
t	Actual thickness of the vault
$\mathrm{W_i}$	Weight of the portion of each block
x_i^{geom}, y_i^{geom}, z_i^{geom}	Coordinates of block's centre of mass
x_j^{geom}, y_j^{geom}, z_j^{geom}	Coordinates of median surface at j interface
x_i^t, y_i^t, z_i^t	Coordinates of the generic point of the thrust surface at the centre of block
x_j^t, y_j^t, z_j^t	Coordinates of the generic point of the thrust surface at the interface